

Long-term sulfate attack on recycled aggregate concrete immersed in sodium sulfate solution for 10 years

L.R. Santillán^a✉, F. Locati^b, Y.A. Villagrán-Zaccardi^a, C.J. Zega^a

a. LEMIT, CONICET, (La Plata, Buenos Aires, Argentina)

b. CICTERRA, UNC-CONICET, (Córdoba, Argentina)

✉ lautarorsantillan@gmail.com

Received 30 April 2019
Accepted 17 September 2019
Available on line 19 February 2020

ABSTRACT: The effect of recycled concrete aggregate (RCA) on concrete performance against external sulfate attack (ESA) is not yet fully known. In this paper, recycled aggregate concretes (RAC) with 0, 50, 75 and 100% of RCA contents were evaluated after 10 years of exposure immersed in 50g/l sodium sulfate solution. Sulfate ingress profiles were obtained by wet chemical analyses and FRX. Also, the mineralogy of the ingress profile was evaluated by thermogravimetric analyses. Finally, microcracking development in samples was evaluated by optical fluorescent microscopy image analysis. Although RAC showed a slight increase in sulfate ingress, due to its higher porosity (about 30% higher SO₃ content near the surface for 50% or higher replacement ratio than control concrete), a dense new matrix still allows a good performance of RAC to external sulfate attack with even 100% RCA content.

KEYWORDS: Concrete; Transport properties; Sulphate attack; Microcracking; Thermal analysis.

Citation/Citar como: Santillán, L.R.; Locati, F.; Villagrán-Zaccardi, Y.A.; Zega, C.J. (2020) Long-term sulfate attack on recycled aggregate concrete immersed in sodium sulfate solution for 10 years. *Mater. Construcc.* 70 [337], e212 <https://doi.org/10.3989/mc.2020.06319>

RESUMEN: *Ataque por sulfatos a largo plazo sobre hormigón de árido reciclado sumergido en solución de sulfato de sodio por 10 años.* El efecto del árido reciclado de hormigón (AR) en el desempeño del hormigón frente al ataque externo por sulfatos (AES) no es aún del todo conocido. En este trabajo, se evaluaron hormigones con áridos reciclados (HAR) con 0, 50, 75 y 100% de AR, tras 10 años sumergidos en solución de sulfato de sodio 50g/l. Se obtuvieron perfiles de ingreso de sulfato mediante análisis químico vía húmeda y FRX. También se evaluó la mineralogía de los perfiles por termogravimetría y la microfisuración mediante microscopía óptica con fluorescencia. Aunque los HAR mostraron un leve incremento en el ingreso de sulfatos debido a su mayor porosidad (aproximadamente 30% más de SO₃ en la superficie para reemplazos de 50% o mayores), una nueva matriz densa permite un aceptable desempeño del HAR frente al AES, aún con un 100% de AR.

PALABRAS CLAVE: Hormigón; Ataque por sulfatos; Propiedades de transporte; Microfisuración; Análisis térmico.

ORCID ID: L.R. Santillán (<http://orcid.org/0000-0002-9040-4417>); F. Locati (<http://orcid.org/0000-0001-9067-1497>); Y.A. Villagrán Zaccardi (<http://orcid.org/0000-0002-0259-7213>); C.J. Zega (<http://orcid.org/0000-0002-9199-9176>)

Copyright: © 2020 CSIC. This is an open-access article distributed under the terms of the Creative Commons Attribution 4.0 International (CC BY 4.0) License.

1. INTRODUCTION

The use of recycled concrete aggregate (RCA) in partial replacement of natural aggregate in concrete production keeps gaining significance in the construction sector due to its economic and environmental implications (1, 2). In the literature, there are plenty of research reports on the mechanical properties of recycled aggregate concrete (RAC). It is well proven that making structural concrete with even 100% of coarse RCA is possible when some considerations are made for the mix design (3–6). Nevertheless, durable properties of RAC are still under investigation due to several concerns, most of which are related to the effect of RCA on concrete porosity. A better knowledge of the durable performance of RAC will allow expanding its possible applications.

The main difference between RCA and natural aggregates (NA) usually used in concrete production is the porosity of each one (7–10). Thus, the use of RCA increases RAC porosity, which is generally higher than natural aggregate concrete (NAC) and depends mainly on the RCA content (11–14). Also, as the pore structure defines the transport properties of concrete, the higher porosity of RCA may lead to a worsened durability performance of RAC. However, the transport properties of concrete are only some of the properties that influence its durability performance. Some positive effects of the use of RCA have been reported as well. For example, in the case of chloride attack, attached mortar in RCA increases the chloride binding capacity (15). Moreover, depending on the moisture condition of RCA at the moment of mixing concrete, its high absorption capacity may reduce the effective water to cement ratio, especially at the level of the interfacial transition zone, resulting in a denser concrete (16–18). This explains why sometimes RAC shows higher flexural or tensile strength than NAC. Likewise, porosity could also imply some beneficial effects regarding durable properties.

The external sulfate attack (ESA) comprises a deleterious process involving a reaction between hydration products of Portland cement and sulfate penetrating from the environment. The rate of deterioration is affected by environmental factors and material properties. This issue is controversial because, although there is much research on the topic, the chemical-physical mechanisms are quite complex. Therefore, there are several parameters involved in ESA kinetics and thermodynamics that are difficult to regard in experimental studies, and to consider in standards and recommendations (19,20).

Regarding environmental factors that affect the ESA process, moisture condition is determinant. If concrete remains saturated, diffusivity is the only mechanism for ions to penetrate the concrete matrix. In this case, the whole range of pore sizes

participates in the transport process, and the damage is only due to the chemical interaction between sulfate ions and cement paste compounds. If concrete is partially saturated, pore solution is found only in finer pores, and this is the only fraction of porosity allowing sulfate penetration. Moreover, if concrete is exposed to wetting and drying cycles, a crystallization salt process takes part in the process, increasing the degree of damage strongly (21–24). When ESA is the sole deterioration process, i.e., when concrete is permanently saturated, so no cycles for salt crystallization are possible, the deterioration mechanism can be described by stages as follows. First, sulfate ingresses from the environment into the concrete matrix by diffusion. Then, a part of this sulfate reacts with cement hydration products (to form ettringite, gypsum or thaumasite, depending on the degree of development of the attack). In this process, a part of sulfate ions is bound by reacting hydration products (mainly AFm phases, hydrogarnet and portlandite), which are depleted. Free sulfate can move forward to a deeper layer to continue the process inwards. The reaction products generate stresses which eventually overcome the tensile strength of concrete and produce cracks that increase the concrete permeability and the sulfate penetration rate. The sulfate is consequently further increased ending up in a vicious cycle. Simultaneously, portlandite depletion reduces the pH of pore liquid and destabilizes C-S-H. This situation is more critical near the surface, where a part of portlandite can be leached as well. At later stages of ESA, the alteration of C-S-H leads to a loose of cohesion in the matrix. In connection with these processes, different zones can be defined from the surface to the bulk of specimens. Each of these layers is defined by particular chemical-physical actions that affect the material. Figure 1 summarizes and describes these four zones: the most external layer, with no portlandite content due to leaching and a disintegrated surface by loss of cohesion due to C-S-H destabilization; a second layer, with a high content of reaction products (mainly gypsum which is more stable than ettringite at high sulfate concentrations) precipitated in cracks previously opened by ettringite crystallization; a third layer with ettringite in formation, opening cracks as a front of attack; and a fourth zone, corresponding to the unaltered bulk (25–27).

The main material properties affecting ESA progression are the concrete permeability and chemical composition, mainly the C_3A content of constituting Portland cement (20,28,29). Therefore, standards point out two main design criteria for producing sulfate-resistant concrete: a maximum limit for the water to cement ratio to get a dense matrix that improves concrete transport properties; and the use of sulfate-resistant cement (with a low C_3A content) to reduce the mineral source for the chemical reaction leading to ettringite formation.

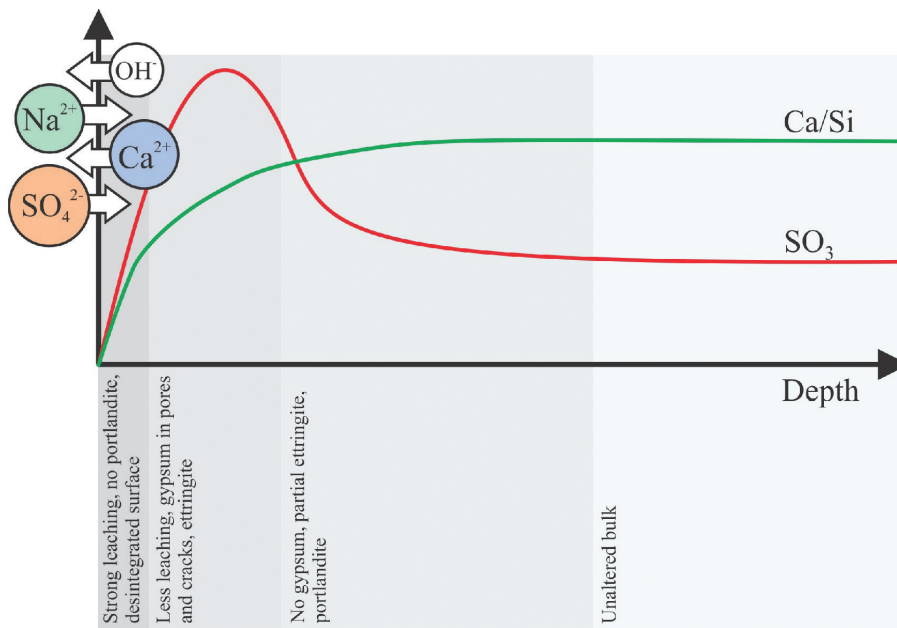


FIGURE 1. Schematic profile of ESA by sodium sulfate solution (adapted from Ref. 25).

There are multiple methods for assessing concrete resistance to sulfate exposure. In general, expansion and loss of compressive strength are the most used methods. Also, mass change and the monitoring of the dynamic modulus of elasticity are applied in some cases. Moreover, different types of microstructural analytical techniques were applied with the focus put on the understanding of ESA mechanisms. These techniques offer the advantage of allowing the assessment of ESA as the external attack it is, i.e., advancing from the surface to the bulk of concrete to construct analyses that describe the development in depth. Complementation of techniques always seems the most convenient approach.

In the case of RAC, both porosity and content of hydration products are modified by using RCA. On the one hand, the attached mortar in RCA particles causes an increment in the total cement past content, which means more content of Portland cement hydration products able to react with external sulfate. On the other hand, as was mentioned above, the use of RCA means increased overall porosity of RAC that translates in higher permeability and might imply an acceleration of ESA kinetics. Furthermore, porosity may also reduce the internal restriction of concrete to deform, and this effect on ESA has been barely considered: ESA damage is mainly due to the formation of expansive products in confined pores. Thus, less internal stresses are generated when more space is available. Moreover, the matrix porosity lessens the stiffness of the whole material. Confinement might be locally reduced as a result, causing lower internal stresses due to

precipitation of ESA products. This hypothesis can explain results from previous studies (30–35), where concretes and mortars made with recycled aggregates showed similar or even better results than mixes with natural aggregates when exposed to the sulfate-laden environment.

The literature regarding RAC performance against ESA is not entirely conclusive. This is mainly due to the several parameters involved in ESA in addition to the specificities related with the use of RCA, which are regarded differently in each study. In general, a worse performance against sulfate attack of RAC than NAC is observed. The detriment is generally linked to the high porosity of RAC. However, there are some studies that present a similar or even better performance for RAC than for NAC. Dhir et al. (36) report no effects of RCA up to a 30% replacement ratio when RAC was exposed to a sulfate solution, and a negative effect only for higher replacement ratios. Bulatovic et al. (37) report a worse performance of 100% RCA concrete than NAC against ESA, but only when the water-cement ratio of RAC was high ($w/c = 0.55$) and a non-sulfate-resistant cement was used. Boudali et al. (38) found better performance against ESA of self-compacting concrete with RCA than NA, and they attribute this result to a high capacity of RCA to relief stresses due to its high porosity. Li et al. (34) and Qi et al. (35) evaluate RAC under combined attack of freeze-thaw and sulfate, and found a better performance of RAC with up to 50% replacement ratio respect to control concretes. There are also several studies in which RAC is enhanced by supplementary

cementitious materials (SCM), chemical admixtures, or other novel constituents, resulting in better performance for RAC than for control concretes. For example, Somna et al. (39) found better results for 100% RCA concrete than for control concrete when 50% of bagasse ash was used as partial replacement of cement. Similar results regarding the benefit of using supplementary cementitious materials (SCM) in RAC are reported in several other studies (40–45). All these results are explained by the reduction in the porosity that SCMs provide to the RAC matrix. For example, Mendivil-Escalante et al. (46) studied the micro-porosity of polyethylene-terephthalate-admixed RAC by several methods, and report a strong reduction in total porosity that may improve the performance against ESA.

1.1. Previous study

A previous study (47) comprises a research program designed to assess the coarse RCA effect on RAC resistance to severe sulfate exposure. With this purpose, four concretes were designed with durability criteria (low w/c and appropriate air entrainment) and different coarse RCA contents. Then, prisms were moulded and half-buried in sulfate-rich soil. These exposure conditions simulate the exposure of ground-level structural elements, where concrete is in contact with sulfate-laden soils and variable moisture and temperature conditions.

Table 1 summarizes the most relevant results of this previous study. In the fresh state, similar concrete slump and a slight variation in air-entrained content with the increment in RCA content is observed. In the hardened state, similar compressive strength for all concretes is observed. Regarding the RACs performance against ESA, after 200 days and 3000 days of exposure, a negligible effect of the RCA content is observed, either by weight variation and dynamic modulus of elasticity. Visual inspection confirms these experimental results and suggests that the new cement matrix of RAC was logically able to mitigate any possible adverse effect of RCA particles embedded in it.

At the same time that prisms for rich-sulfate soil exposure were casted, other prisms were moulded to

be immersed in sulfate solution, i.e., in a saturated condition. After 10 years of exposure these specimens were evaluated to assess the RCA influence on solely external sulfate attack process. This paper presents an extended profile assessment of the ESA on these RACs by multiple instrumental analyses.

2. EXPERIMENTAL

2.1. Materials and mixes

The used binder was a moderately sulfate resisting blended Portland cement, according to IRAM 50001:2010 (48), containing 12% w/w blast furnace slag and 18% w/w limestone filler. This cement is comparable in composition to a CEM II/B-M (L-S) 42.5 N according to EN 197-1 (49) produced with a sulfate resisting clinker. Natural aggregates were two river siliceous sands, a fine sand (FS) and a coarse sand (CS). Also, two crushed granite aggregates (CG) with maximum sizes of 19 and 25 mm were used. Recycled concrete aggregate (RCA) was obtained from crushed conventional concretes with variable and unknown characteristics and the only common features being that, all of them corresponded to structural concrete (with compressive strength above 21 MPa) and contained crushed granite as coarse aggregate. The crushing of concretes was carried out by two size lab-scale sized jaw crushers. The maximum size of RCA was 25 mm. Particle size distribution was determined following ASTM C136 (50). To obtain coarse and fine aggregates that satisfy the limits established by ASTM C33 (51), FS and CS were combined in proportions of 20%-80%, respectively, of the total fine aggregate, and CG-19 and CG-25 in proportions of 20%-80%, respectively, of the total coarse aggregate. Figure 2 shows the particle size distributions of the resulting fine and coarse natural aggregates, RCA, and limits established by ASTM C33. In Table 2, evaluated properties of all aggregates are presented, including maximum size and fineness modulus, density in saturated surface-dry condition and water absorption capacity (ASTM C127) (52), content of material finer than 75 μm (ASTM C117) (53), and Los Angeles abrasion loss (ASTM C131) (54).

TABLE 1. Highlighted results of previous study (47).

Concrete	Fresh state properties		Compressive strength (MPa)	Sulfate exposure			
				Weight variation (g)		Dynamic modulus of elasticity (GPa)	
	Slump (mm)	Air-entrained content (%)		200 days	3000 days	200 days	3000 days
R-0	120	5.0	33.3	78	85	41	42
R-50	110	4.7	32.5	90	80	40	41
R-75	100	5.1	33.3	100	85	38	40
R-100	100	4.2	36.5	105	90	38	40

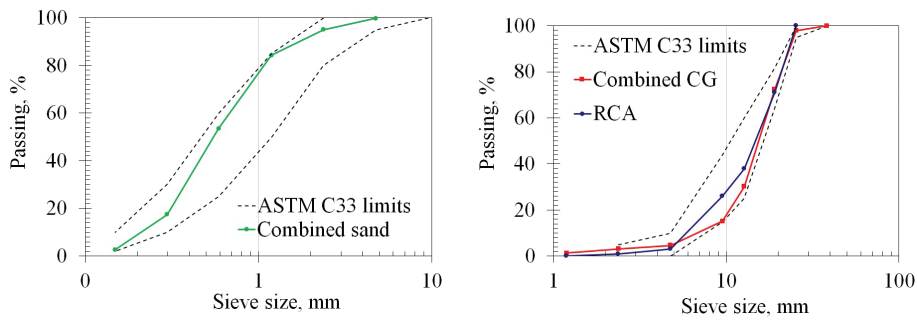


FIGURE 2. Particle size distribution of aggregates.

TABLE 2. Properties of aggregates.

Properties	FS	CS	CG	RCA	
Maximum size (mm)	-	-	25	19	25
Fineness modulus	1.66	2.67	7.44	6.83	6.99
Density ssd (g/cm ³)	2.52	2.60	2.69	2.65	2.44
Particles passing 75 µm sieve (%)	1.51	0.70	0.40	0.55	0.10
Absorption (%)	0.80	0.20	0.30	0.40	4.70
Los Angeles abrasion loss (%)	-	-	25.7	28.0	41.4

TABLE 3. Proportions of RACs.

Materials	Content of RCA (%)			
	R-0	R-50	R-75	R-100
Water (kg)	145	145	145	145
CEM II/B-M (L-S) 42.5 N (kg)		422		
FS (kg)		157		
CS (kg)		627		
CG 19 mm (kg)	195	95	48	-
CG 25 mm (kg)	791	397	197	-
RCA (kg)	-	451	674	897
Air-entraining admixture (l)		0.126		

With the aim of knowing the effects of different contents of coarse RCA on ESA resistance, concrete mixes were designed with 0, 50, 75 and 100% of replacement v/v of NA by RCA. In addition, to comply with durability criteria for sulfate-laden environments, and determine any detrimental effect of the replacement of NCA by RCA on the performance of concrete, mixes were designed with a water/cement ratio of 0,35 and air-entrainment admixture was used. Table 3 presents the proportions of mixes, where the designation of each concrete mix corresponds with its RCA content. To avoid a variation in the effective water/cement ratio of fresh concrete, RCA was pre-saturated in water and then superficially dried. Thus, RCA were used in saturated and surface dry condition (SSD).

For sulfate testing, 75 × 150 × 250 mm prisms were cast. To evaluate transport properties of RACs, 75 × 75 × 300 mm prisms for sorptivity (according to IRAM 1871 (55)), and 200 mm cubes for water penetration under pressure tests (according to IRAM 1554 (56), equivalent to EN 12390-8 (57)), were also cast. All samples were cured for 28 days in a humid chamber. Before testing, 75 × 75 × 300 mm prisms were sawed to obtain 50 × 75 × 75 mm prismatic specimens to evaluate the sorptivity of concrete. Moreover, density, porosity, and water absorption were evaluated with the remaining parts of the specimens, following ASTM C642 (58).

2.2. Sulfate exposure and analytical techniques

Prismatic specimens of 75 × 150 × 250 mm were covered with waterproof paint on all faces excepting the casting face of 75 × 250 mm. These specimens were submerged in 50 g/l sodium sulfate solution maintained at 23±3°C, with a solution/concrete volume ratio of 4 and without periodic solution refreshing. After 10 years of exposure, sulfate ingress was assessed in portions of the specimens by collecting powder samples by dry progressive profiling with a diamond tool, at increasing depths from the exposure face of 0-3 mm, 3-6 mm, 6-10 mm, 10-15 mm, 15-20 mm, and 20-30 mm. The powder samples were collected simultaneously as the tool was advancing. The sampling area in all cases was larger than 20 cm². Then, RAC powder samples

were homogenized by grinding them with mortar and pestle up to all the material passed through a 75 μm sieve.

Chemical analysis (CA), X-ray fluorescence (XRF), and TGA/DTA were performed on fractions of the powder samples for obtaining the chemical and mineralogical compositions at different depths. Chemical compositions of the powder samples were determined by wet analysis and X-ray fluorescence (XRF). For wet analysis, the sample was dissolved with hydrochloric acid, and the insoluble residue was eliminated by filtration. Then, sulfate was precipitated as barium sulfate after the addition of barium chloride solution. The precipitate was collected by filtration, calcined, and weighed to compute sulfate contents expressed as SO_3 . XRF analyses were made with an Ametek Spectro IQ II. TGA/DTAs were conducted in a previously ground and homogenised samples of 0.05 g, at a heating rate of 10°C/min (59), up to 1050°C under an inert atmosphere of N_2 .

To analyse the damage in the specimens, 75 mm \times 150 mm slices were taken for microscopic observations. The sampling direction was such that the whole cracking pattern from the surface to the inner layers could be observed. These samples were impregnated with fluorescent resin (epoxy resin with sodium fluorescein) and polished to obtain thin slices. Images were taken at 1.5, 4.5, 8, and 25 mm, covering an area of 2.7 \times 14 mm on each depth.

3. RESULTS AND DISCUSSION

3.1. Physical and transport properties

Table 4 presents physical properties of RACs. In accordance with the literature, water absorption and porosity of RAC increase with a higher RCA content (7,10,13,14). This effect is connected with the porosity of the attached mortar in RCA particles. Density of RACs decreases with RCA content, due to the higher porosity of recycled aggregates than natural aggregates.

Transport properties are also presented in Table 4. Sorptivity values increase with the RCA content. This suggests that the sorptivity coefficient is affected by all the pore range of RAC resulting from the summation of the attached mortar and the new cement

matrix. However sorptivity have a slight slope from R-75 to R-100, which suggest that the effect of RCA content could be overlapped by differences in the new cement matrix. Compressive strength and air-entrained content values for R-100 concrete suggest a relative denser matrix than other RACs.

Conversely, the average water penetration under pressure was relatively low for all concretes (below 30 mm, which is the maximum limit value accepted for concrete exposed to a high sulfate-laden environment by Argentine Regulations (60)), with a slight decrease of the water penetration when the RCA content increased. In this case, the higher porosity of RAC caused by the attached mortar on RCA particles showed no adverse effect on the water penetrability under pressure. These results may appear inconsistent with the overall porosity values of each concrete mix. However, considering that only coarse RCA was used, the influence of this constituent on the porosity of the most external layer of 15-20 mm is normally limited, and this seems to be reflected by the results of water penetration under pressure.

3.2. Visual aspect and microscopic observations

Figure 3 shows the pictures of specimen 75 \times 150 mm cross-section, with the ingress face on the top for each picture. After 10 years of exposure in high concentration sodium sulfate solution, all specimens seems to have a good state, with no visual signs of deterioration, even for the specimens with 100% v/v RCA content. This is in accordance with the results of the previous study (47), where no detrimental effect of RCA content on the performance of recycled concretes specimens semi-buried in sulfate soil was observed.

The evaluation of the damage in RACs is presented in Figure 4, corresponding to the images from epifluorescent optical microscopy taken from the four concrete specimens. From left to right, each image shows the layers from the surface to the bulk, centered at 1.5, 4.5, 8 and 25 mm from the surface. A common micro-cracking pattern is observed for all mixes at all depths, with a morphology non-related to ESA deterioration mechanisms reported in bibliography. This low level of micro-cracking can be connected with the affectation of samples due to drying or the preparation of thin slices.

TABLE 4. Physical and transport properties of RACs.

Properties	R-0	R-50	R-75	R-100
Absorption (%)	4.6	5.3	5.8	6.3
Porosity (%)	10.4	12.8	12.7	13.4
Density (kg/m^3)	2.27	2.21	2.18	2.14
Sorptivity ($\text{g/m}^2 \cdot \text{seg}^{1/2}$)	3.8	3.8	4.7	4.2
Average water penetration under pressure (mm)	20 (2.4)	18 (3.8)	15 (1.6)	16 (2.9)

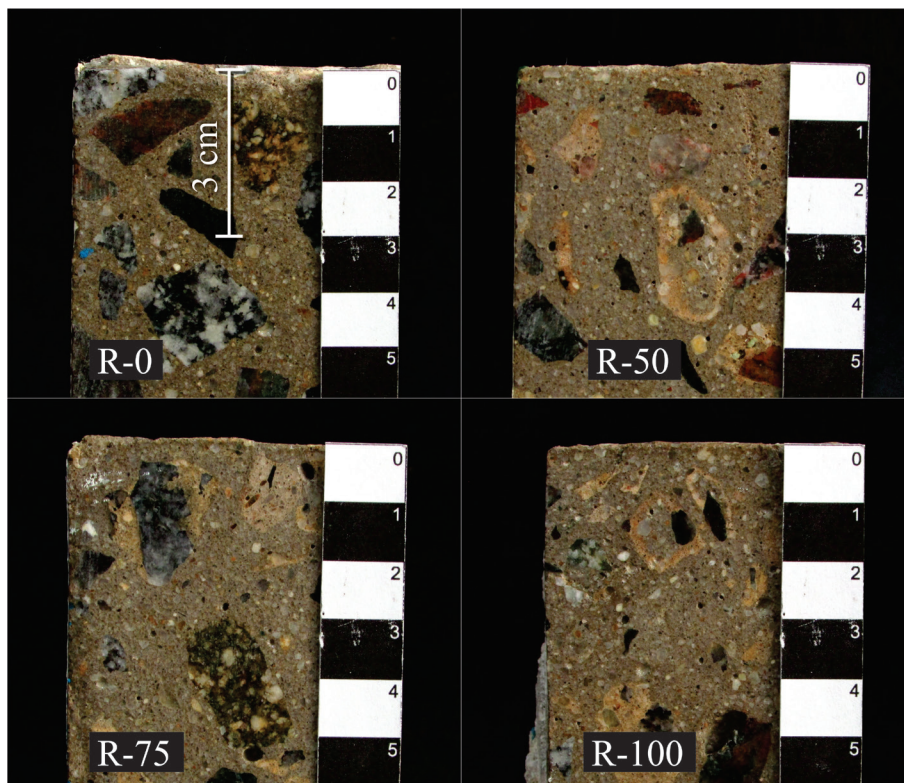


FIGURE 3. Visual observation of specimens after 10 years of exposure.

More importantly, cracking development is notorious for the first depth for R-0 and R-100 and it is present over the entire field of these images. The morphology of these cracks, which develop edging natural aggregate particles, is parallel to the surface and consistent with damage due to ESA reported in bibliography (61–63). For R-50, small cracks are observed only at the top of the image, whereas for R-75 no cracking that could be associated with ESA was detected. These results suggest that, although it is possible that sulfate penetrated into the concrete matrix and precipitated as ESA products, the developed internal stresses were not enough to exceed the RACs tensile strength levels, with exception of the first layers. Thereby, a good performance of all RACs against ESA regardless of the RCA content is observed. With small disparities, microscopic observations show a better behaviour of R-75, followed by R-50, and the worse performance corresponding to R-0 and R-100 concretes. This ambiguous effect of RCA on RAC resistance has been previously reported in bibliography (31,34,38).

3.3. Incoming sulfate

Results of wet CA, XRF, and average values between both are presented in Figure 5 for each concrete mix. The reported SO_3 contents are the

summation of the sulfate contained in the constituting cement and attached mortar in RCA, the sulfate contained in ESA products, and the free sulfate in the pore solution at the moment of sampling (which precipitated as salt crystals when specimens were dried). The second depth (3 to 6 mm) has a higher sulfate content than the surface layer (0 to 3 mm) for all concretes. This outcome is in agreement with other studies on ESA mechanisms (20,26,63), which is usually explained by the presence of a densification zone in which a large amount of ESA products precipitate and reduce porosity. In Figure 5, a slight increment in the sulfate content at the second depth with increasing RCA content (from 1.63% for R-0 to 2.18% for R-100) is noted, but this increment is not proportional to the RCA content (2.10% and 1.93% for R-50 and R-75 respectively) (Table 5). Although each pair of full penetration profiles determined by both analytical techniques are consistent, these profiles are not in relation with the RCA content in concrete. The total amount of incoming sulfate can be computed as the integral of the SO_3 contents over the depth. The results in Table 5 show that R-0 and R50 have the smallest amount of incoming sulfate, followed by R-100 with an intermediate value, while R-75 has the highest content (about a 30% more SO_3 content than control concrete).

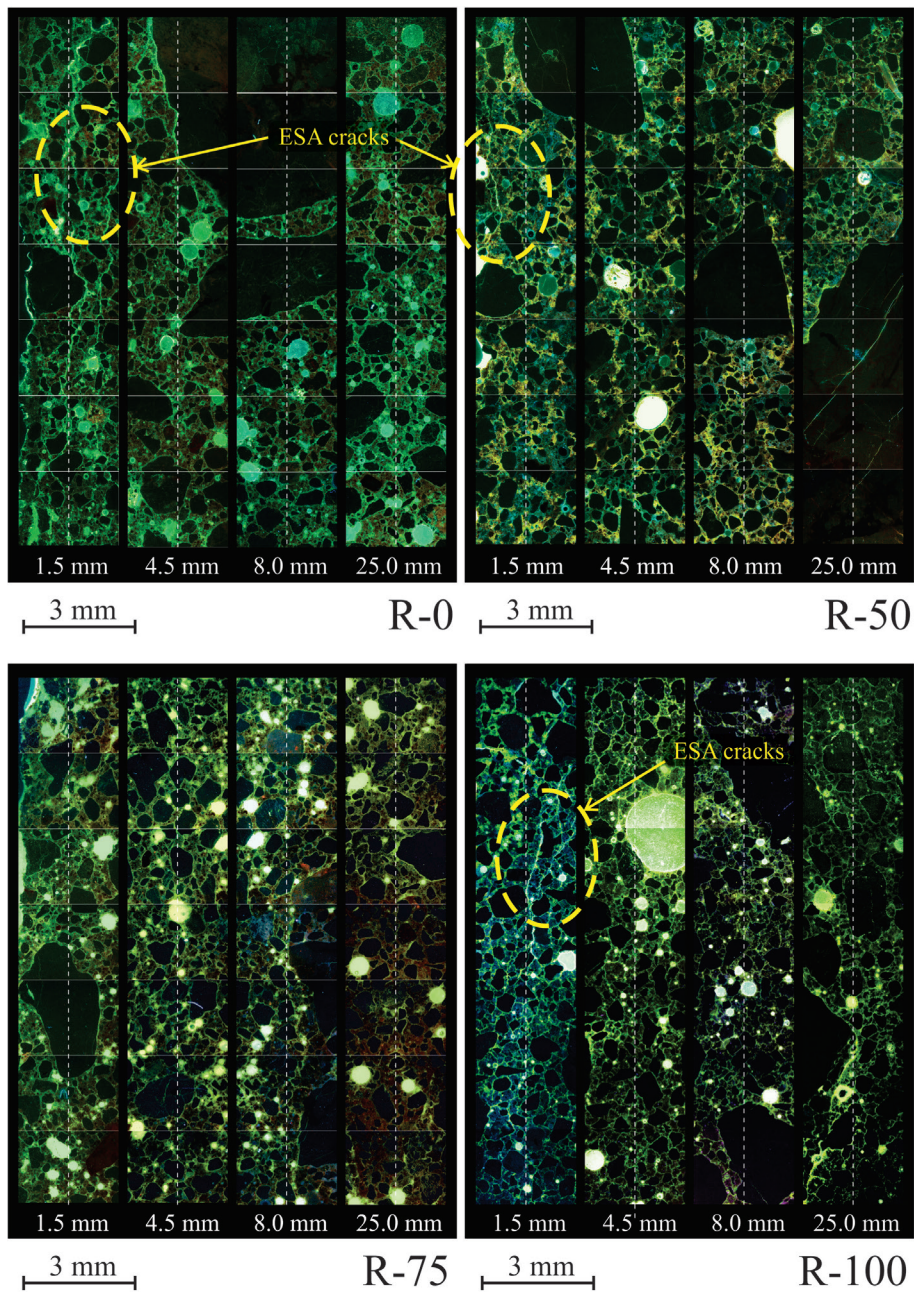


FIGURE 4. Optical fluorescent microscopy images.

3.4. Thermal analyses

Figure 6 presents the results of thermogravimetry (TG). Each subfigure presents the samples at different depths for each concrete mix, referenced with increasing numbers from 1 to 6 for the increasing depths (0-3 mm, 3-6 mm, 6-10 mm, 10-15 mm, 15-20 mm, 20-30 mm). The weight loss at a certain temperature is certainly originated by the summation of the contributions of more than one compound, but the presence of different compounds

can be inferred from the identification of peaks in the DTG pattern which show characteristic weight loss temperature for different compounds (64). Therefore, the observed peaks in the derivative TG patterns (DTG) indicate the presence of free water, ettringite, gypsum, portlandite, calcite, and decomposition of sulfates, at approximate temperatures of 50, 100, 120, 420, 650, and over 750°C, respectively. These compounds are indicated in Figure 6 for identification purposes only and quantitative analysis was done only for calcite as explained below. The

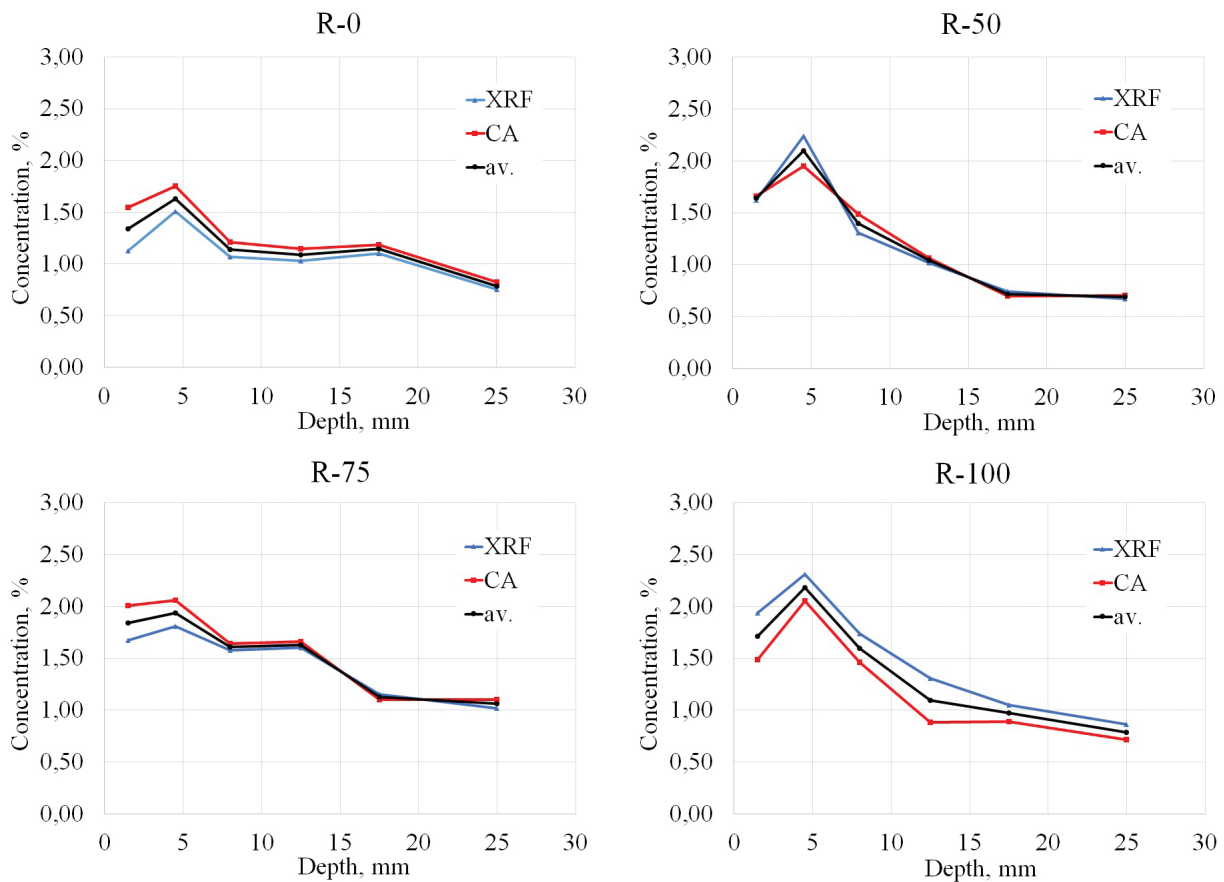


FIGURE 5. Sulfate profiles of RACs determined by CA and XRF.

TABLE 5. Maximum and total incoming SO₃.

RAC	R-0	R-50	R-75	R-100
Maximum SO ₃ content	1.63	2.10	1.93	2.18
SO ₃ indexes (%·cm)	3.27	3.28	4.21	3.63

decomposition of sulfates usually takes place at much higher temperatures, but the mix with compounds like alumina or silica seems to reduce this temperature quite significantly (65).

Figure 7 presents the profiles for the ratios between the calcium contained in calcite (determined by integration of the corresponding peaks in the DTG patterns applying the tangent method for discounting the contribution of other phases (64)), and the total calcium content (determined by XRF). All samples show noticeable calcite contents as all mixes were prepared with a limestone blended cement. Additional calcite is provided by partially carbonated cement paste contained in RCA, and, therefore, R-50, R-75, and R-100 show an increased calcite content in relation to R-0. However, the most external layers of all series contained even higher calcite contents and also depletion of portlandite. This

is indicative of the carbonation of these samples. Portlandite is also consumed with the formation of gypsum, which is also mostly detected for the outer layers. The portlandite depletion and the reduction in pH due to carbonation reduce the stability of C-S-H and contribute to the progression of its decalcification (66–68). The significant amount of calcite noted for all concretes in the most external depth is higher than the potential maximum amount corresponding to the full carbonation of portlandite. After complete portlandite depletion to form calcite, gypsum, and ettringite, additional Ca⁺⁺ ions are made available for calcite formation by progressive decalcification of the C-S-H phase. This process is sometimes regarded as carbonation of C-S-H, but the contribution of sulfate to the progress of the process should also be taken into account.

Regarding ESA products, on the one hand, ettringite was identified in all concretes at all depths. This situation evidences that sulfate ions penetrated into the concrete matrix and precipitated in combination with C₃A hydrates. The precipitation of products and the associated internal stresses seem to be insufficient to overcome the tensile strength of RACs. R-0 and R-75 present the highest amounts of

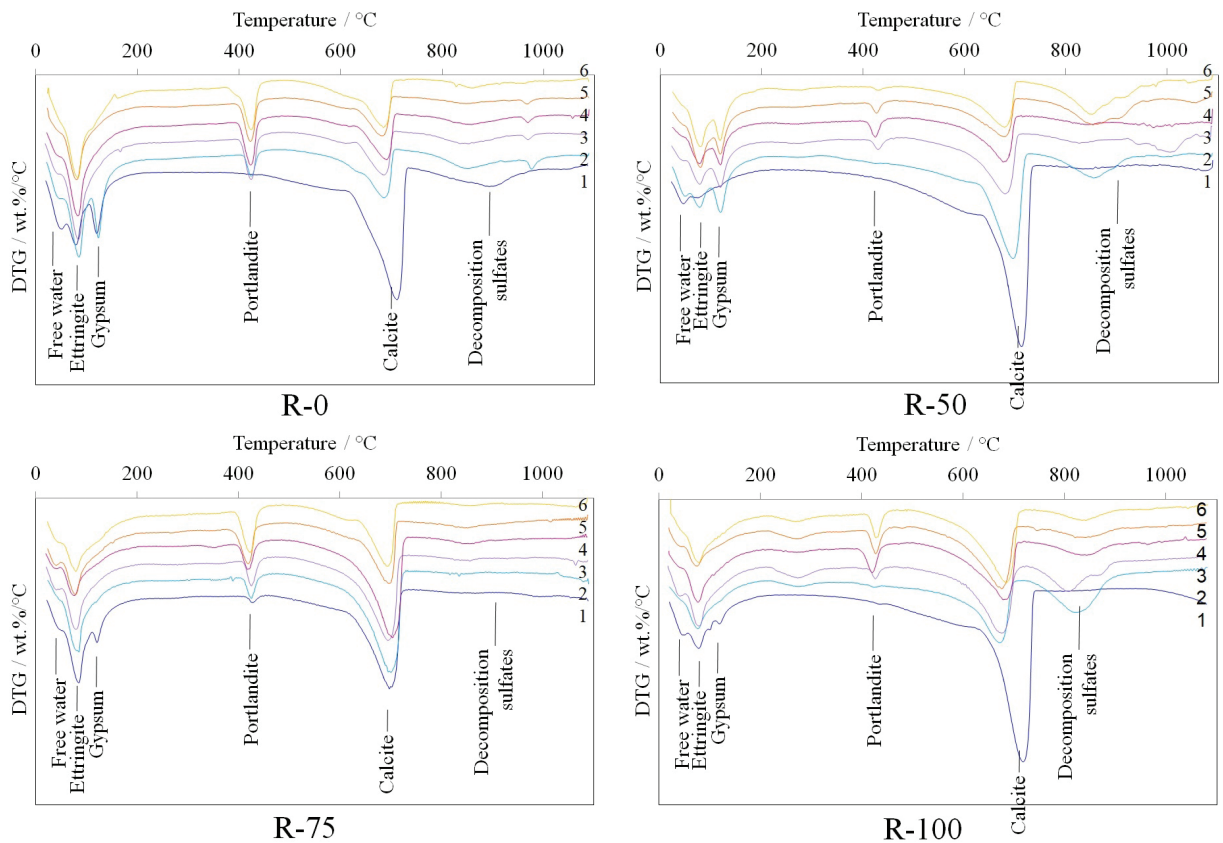


FIGURE 6. DTG patterns for samples at different depths of concretes.

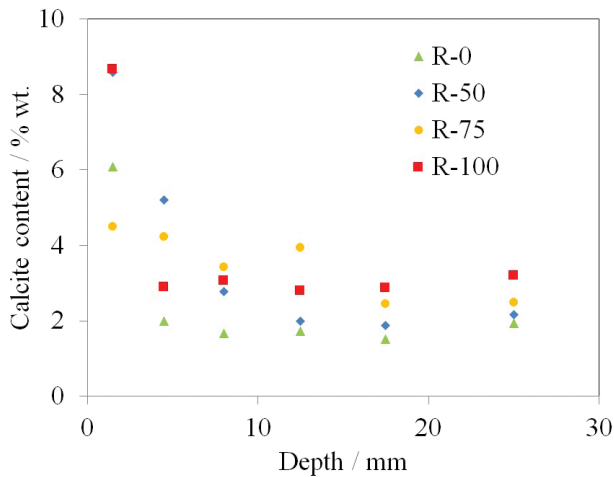


FIGURE 7. Calcite profiles computed from TG/DTA.

ettringite on surface layers. On the other hand, gypsum appears only near the surface, except in the case of R-50 for which significant amounts of gypsum were found for all layers. At first, it is expected that ettringite would evolve into gypsum, as the latter is a more thermodynamically stable phase at high SO_3

concentrations. However, ettringite is possibly stabilized due to a high concentration of sodium (69,70), so both phases are found simultaneously even after long periods of exposure and after the development of cracking. Finally, some free sulfate is suggested by thermogravimetry in some samples, as precipitates of mirabilite or thenardite during the drying process.

Although all concretes mixes showed an acceptable performance (little development of cracking) and small differences regarding the amounts of bound sulfate, the mineralogical profiles show that the ESA mechanism was not the same for all the specimens. For R-0, ettringite is observed over the entire profile, whereas gypsum is present only near the surface, in coincidence with the cracking detected by microscopy. For R-50, gypsum is observed throughout the profile, which suggests a process of conversion of ettringite into gypsum. As no significant cracking is observed in this concrete, it is possible that the porosity of the matrix allowed the precipitation of formation products with no generation of internal stresses. In the case of R-75, only a small amount of gypsum is observed near the surface and ettringite in all depths. R-75 is actually more porous than R-50, but the results from

the sulfate penetration profile revealed a higher apparent diffusivity in R-50 than in R-75, and, therefore, more significant precipitation of gypsum is expected in the former. In these two concretes, precipitation of formation products is confirmed, but this is apparently insufficient for the development of cracking due to a low internal restriction to deformation with respect to control concrete. For R-100, ettringite is observed at all the analyzed depths in superposition with significant contents of free sulfate. In this case, cracking seems to allow faster sulfate penetration, which was not bound as gypsum at the moment of sampling. The reason for this situation is not totally clear. The thermogravimetry patterns also show a bump near 300 °C, which can be attributed to the presence of strätlingite (which is similar to AFm but with a specific silica content). The differences in the mineralogical outcome of the analyses describe slightly different mechanisms in the deterioration process by ESA occurring in each concrete, which can be connected with the different internal restriction of concretes in each mix.

3.5. Internal restriction hypothesis

The R-0 mix had the lowest porosity among the studied mixes. Cracking and elevated gypsum content near the surface was consistently detected. The SO₃ content reaching the bulk is lower than in the other mixes in connection with its reduced pore structure. The higher internal restriction to deform makes this concrete more prone to the development of internal stresses and cracks than the other series, for the same amount of reaction products being formed. The observation of significant cracking confirms this situation, and partially explains certain acceleration in the sulfate penetration rate and high contents of ettringite in depth. The portlandite contents at high depths are consistent with stable hydration products despite the exposure to sulfate (third zone from the surface in Figure 1).

For the R-50 and R-75, results are mostly in relation with the resulting porosity of each concrete. The increased porosity due to the inclusion of RCA is reflected in higher SO₃ contents near the surface, but the situation becomes more complex for the deeper layers. Even though R-50 shows lower SO₃ contents in internal layers, a high content of gypsum was also found. Conversely, R-75 shows higher contents of SO₃ in the inner layers than R-50 and a high content of ettringite near the surface. The presence of unaltered portlandite in the depth confirms a reduction in the transport rate as a consequence of precipitation of formation products. The porosity of the material seems to show an optimal balance between the sulfate penetration rate and the product formation rate. This is in agreement

with other studies where the formation of ESA products seems to have a beneficial effect in some mixes, where porosity is being reduced and internal stresses does not reach the tensile strength of concrete (34,45). With additional ingress of sulfate, it is expected that internal stresses will continue increasing and cracking will progress. Whereas this situation seems to be the case for R-100, which demonstrated a much faster sulfate penetration rate, R-50 apparently needed less incoming sulfate for development of cracking due to its comparatively low porosity and greater internal restriction to deform.

With the highest content of RCA, R-100 shows significant development of cracking at the surface, similarly to R-0 in the opposite situation regarding RCA content. In this concrete, significant content of ettringite at middle depths and high contents of gypsum and calcite near the surface were found. Significant amounts of free sulfate were also found, suggesting fast ingress of sulfate due to the formation of cracks. The benefit of the lower internal restriction due to the porosity of R-100 seems to be less important than the increase in the sulfate penetration rate. As large amounts of calcite are also found, there seems to be a competition for the consumption of portlandite, and being the sulfate the last arriving, the precipitation of gypsum would only be possible by decalcification of C-S-H, which is a less direct process.

Moreover, the balance of the effects of increased porosity, decreased internal restriction of concrete to deform, and increased sulfate penetration rate, could depend on the particular features of the test, either mix properties (e.g. porosity of aggregate, w/c of the new matrix) or exposure conditions (e.g. moisture conditions, sulfate concentration, etc.). For example, the complexity of the impact of highly porous aggregates is exemplified by the work of Lee et al (30), where mortar containing variable contents of fine recycled aggregate was exposed in high concentration sodium sulfate solution. Replacement ratios of 25 and 50% resulted in lower expansion than the one of control mortar, while 75 and 100% replacement ratios resulted in more substantial expansion than in the control mortar. In this case, 50% was the optimal fraction of recycled aggregate to minimize bars deformation under that ESA conditions.

Regarding the transport properties assessed in RACs, Figure 8 shows the relationship between the incoming sulfate and both transport properties assessed in RACs (sorptivity and depth of water penetration under pressure). Sorptivity seems to correspond better with the performance of RACs against this condition of ESA than the water penetration depth. As mentioned above, sorptivity seems to be related to the porosity of the new cement matrix besides the RCA content.

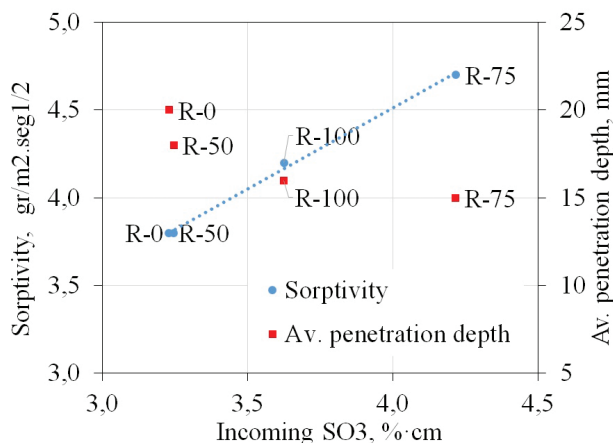


FIGURE 8. Incoming SO₃ and transport properties.

4. CONCLUSIONS

In this study, the effect of coarse recycled concrete aggregate (RCA) content on the physical and transport properties, and also on the deterioration process of recycled concrete immersed for 10 years in sodium sulfate solution were assessed. Sorptivity and water penetration, as well as sulfate ingress profiles, cracking, and mineralogical composition were analyzed at different depths in each concrete specimen after the exposure period. The following outcomes can be stated:

- RCA content increases the general porosity of recycled concrete, which is reflected in transport properties, such as water absorption and sorptivity, whereas water penetration shows its own trend. On the one hand, water penetration seems to be governed by the new cement matrix with little impact of the physical properties of the type of coarse aggregate. On the other hand, sorptivity is more affected by the RCA content, but the relative impact is only a fraction of that on the total porosity.
- Regarding RACs performance against ESA, visual inspection and microscopic observations of specimens showed acceptable condition for all samples. A cracking developed due to ESA was only observed in superficial layers, regardless of RCA contents.
- Although RCA allows a higher incoming sulfate and ESA products precipitation, there is not a direct relation with the cracking level observed. Ettringite and gypsum precipitation suggested a situation of ESA in progress that might eventually develop in some cracking.
- The increased porosity provided by RCA plays an ambiguous role in the ESA mechanism. On the one hand, it increases the sulfate penetration rate, mostly observed near the surface of

specimens. On the other hand, damage can only be possible due to the generation of cracking as a consequence of internal stresses, and stresses are not produced when there is sufficient space for precipitation of reaction products, or a lower stiffness of whole material. The balance of both effects suggests a certain optimal content of RCA for improved ESA resistance.

- The results presented in this paper confirm that when RAC is designed with a high quality new cement matrix, the influence of RCA content on ESA resistance is indiscernible in laboratory conditions.

ACKNOWLEDGMENTS

This work was partially funded by FONCyT, ANPCyT through the project grant PICT 2015-3339 Prest BID. The constructive criticism of members of the RILEM TC 251-SRT on Sulfate Resistance Testing as well as the one from anonymous reviewers is also greatly appreciated.

REFERENCES

1. Hansen, T.C. (1986) Recycled aggregates and recycled aggregate concrete second state-of-the-art report developments 1945–1985. *Matériaux et Constructions*. 19 [111], 201–246. <https://doi.org/10.1007/BF02472036>.
2. Abbas, A.; Fathifazl, G.; Isgor, O.B.; Razaqpur, G. (2006) Environmental benefits of green concrete. *EIC Climate Change Conference 2006 IEEE; 10–12 May 2006*. 1–8. <https://doi.org/10.1109/EICCCC.2006.277204>.
3. Zega, C.J.; Di Maio, A.A. (2007) Efecto del agregado grueso reciclado sobre las propiedades del hormigón. *Bolet. Téc. IMME*. 45 [2], 1–11.
4. Etxeberria, M.; Vázquez, E.; Mari, A.; Barra, M. (2007) Influence of amount of recycled coarse aggregates and production process on properties of recycled aggregate concrete. *Cem. Conc. Res.* 37 [5], 735–742. <https://doi.org/10.1016/j.cemconres.2007.02.002>.
5. Kou, S.C.; Poon, C.S. (2013) Long-term mechanical and durability properties of recycled aggregate concrete prepared with the incorporation of fly ash. *Cem. Concr. Comp.* 37 [1], 12–19. <http://dx.doi.org/10.1016/j.cemconcomp.2012.12.011>.
6. Poon, C.S.; Shui, Z.H.; Lam, L. (2004) Effect of microstructure of ITZ on compressive strength of concrete prepared with recycled aggregates. *Const. Build. Mat.* 18 [6], 461–468. <https://doi.org/10.1016/j.conbuildmat.2004.03.005>.
7. Gómez-Soberón, J.M.; Agulló, L.; Vázquez, E. (2002) Cualidades Físicas y Mecánicas de los Agregados Reciclados de Concreto. Aplicación en Concretos. *Tecnología y construcción*. XIII–157, 10–22.
8. Sánchez de Juan, M.; Alaejos Gutiérrez, P. (2009) Study on the influence of attached mortar content on the properties of recycled concrete aggregate. *Const. Build. Mat.* 23 [2], 872–877. <https://doi.org/10.1016/j.conbuildmat.2008.04.012>.
9. Nixon, P.J. (1978) Recycled concrete as an aggregate for concrete—a review. *Matériaux et Constructions*. 11 [65], 371–378. <https://doi.org/10.1007/BF02473878>.
10. Gómez-Soberón, J.M. (2003) Relationship between gas adsorption and the shrinkage and creep of recycled aggregate concrete. *Cem. Concr. Aggeg.* 2, 42–48. <https://doi.org/10.1520/CCA10442J>.
11. Thomas, C.; Setián, J.; Polanco, J.A.; Alaejos, P.; Sánchez de Juan, M. (2013) Durability of recycled aggregate concrete. *Const. Build. Mat.* 40, 1054–1065. <https://doi.org/10.1016/j.conbuildmat.2012.11.106>.

12. Gómez-Soberón, J.M. (2002) Porosity of recycled concrete with substitution of recycled concrete aggregate. An experimental study". *Cem. Conc. Res.* 32, 1301–1311. [https://doi.org/10.1016/S0008-8846\(02\)00795-0](https://doi.org/10.1016/S0008-8846(02)00795-0).
13. Gonçalves, A.; Esteves, A.; Vieira, M. (2004) Influence of recycled concrete aggregates on concrete durability, *International RILEM Conference on the Use of Recycled Materials in Building and Structures, 8–11 November, Barcelona, Spain.* 554–562.
14. Olorunsogo, F.T.; Padayachee, N. (2002) Performance of recycled aggregate concrete monitored by durability indexes. *Cem. Conc. Res.* 32 [2], 179–185. [https://doi.org/10.1016/S0008-8846\(01\)00653-6](https://doi.org/10.1016/S0008-8846(01)00653-6).
15. Villagrán-Zaccardi, Y.A.; Zega, C.J.; Di Maio, Á.A. (2008) Chloride Penetration and Binding in Recycled Concrete. *J. Mat. Civil Eng.* 20 [6], 449–455. [https://doi.org/10.1061/\(ASCE\)0899-1561\(2008\)20:6\(449\)](https://doi.org/10.1061/(ASCE)0899-1561(2008)20:6(449)).
16. Etxeberria, M.; Vázquez, E.; Mari, A. (2006) Microstructure analysis of hardened recycled aggregate concrete. *Mag. Conc. Res.* 58 [10], 683–690. <https://doi.org/10.1680/macrc.2006.58.10.683>.
17. Otsuki, N.; Miyazato, S.; Yodsudjai, W. (2003) Influence of Recycled Aggregate on Interfacial Transition Zone, Strength, Chloride Penetration and Carbonation of Concrete. *J. Mat. Civil Eng.* 15 [5], 443–451. [https://doi.org/10.1061/\(ASCE\)0899-1561\(2003\)15:5\(443\)](https://doi.org/10.1061/(ASCE)0899-1561(2003)15:5(443)).
18. Medina, C.; Frías, M.; Sánchez de Rojas, M.I. (2012) Microstructure and properties of recycled concretes using ceramic sanitary ware industry waste as coarse aggregate. *Const. Build. Mat.* 31, 112–118. <https://doi.org/10.1016/j.conbuildmat.2011.12.075>.
19. Neville, A. (2004) The confused world of sulfate attack on concrete. *Cem. Conc. Res.* 34 [8], 1275–1296. <https://doi.org/10.1016/j.cemconres.2004.04.004>.
20. Menéndez-Mendez, E.; Matschei, T.; Glasser, F.P. (2013) Sulfate Attack of Concrete. In *Performance of Cement-Based Materials in Aggressive Aqueous Environments*, RILEM. Springer. 8–74. https://doi.org/10.1007/978-94-007-5413-3_2.
21. Haynes, H.; O'Neill, R.; Mehta, K.P. (1996) Concrete Deterioration from Physical Attack by Salts. *Concrete International*. 18, 63–68.
22. Scherer, G.W. (2004) Stress from crystallization of salt. *Cem. Conc. Res.* 34 [9], 1613–1624. <https://doi.org/10.1016/j.cemconres.2003.12.034>.
23. Stark, D. (1989) Durability of Concrete in Sulfate-Rich Soils. *Research and Development Bulletin RD097, Skokie, Illinois: Portland Cement Association.* 14p.
24. Xiao, Q.H.; Li, Q.; Cao, Z.Y.; Tian, W.Y. (2019) The deterioration law of recycled concrete under the combined effects of freeze-thaw and sulfate attack. *Const. Build. Mat.* 200, 344–355. <https://doi.org/10.1016/j.conbuildmat.2018.12.066>.
25. Whittaker, M.; Black, L. (2015) Current knowledge of external sulfate attack. *Adv. Cem. Res.* 27 [9], 532–545. <https://doi.org/10.1680/adcr.14.00089>.
26. Santhanam, M.; Cohen, M.D.; Olek, J. (2003) Mechanism of sulfate attack: a fresh look. Part 2: Proposed mechanisms. *Cem. Conc. Res.* 33 [3], 341–346. [https://doi.org/10.1016/S0008-8846\(02\)00958-4](https://doi.org/10.1016/S0008-8846(02)00958-4).
27. Irassar, E.F.; Bonavetti, V.L.; González, M. (2003) Microstructural study of sulfate attack on ordinary and limestone Portland cements at ambient temperature. *Cem. Conc. Res.* 33 [1], 31–41. [https://doi.org/10.1016/S0008-8846\(02\)00914-6](https://doi.org/10.1016/S0008-8846(02)00914-6).
28. Collepardi, M. (2003) A state-of-the-art review on delayed ettringite attack on concrete. *Cem. Conc. Comp.* 25 [4-5 SPEC], 401–407. [https://doi.org/10.1016/S0958-9465\(02\)00080-X](https://doi.org/10.1016/S0958-9465(02)00080-X).
29. Metha, K.P.; Monteiro, P.J.M. (2006) Concrete: Microstructure, Properties and Materials, Third Edit. McGraw-Hill, New York, (2006).
30. Lee, S.; Swamy, R.N.; Kim, S.; Park, Y. (2008) Durability of Mortars Made with Recycled Fine Aggregates Exposed to Sulfate Solutions, *J. Mat. Civil Eng.* 20 [1], 63–70. [https://doi.org/10.1061/\(ASCE\)0899-1561\(2008\)20:1\(63\)](https://doi.org/10.1061/(ASCE)0899-1561(2008)20:1(63)).
31. Lee, S. (2009) Influence of recycled fine aggregates on the resistance of mortars to magnesium sulfate attack. *Waste Manag.* 29 [8], 2385–2391. <https://doi.org/10.1016/j.wasman.2009.04.002>.
32. Boudali, S.; Kerdal, D.E.; Ayed, K.; Abdulsalam, B.; Soliman, A.M. (2016) Performance of self-compacting concrete incorporating recycled concrete fines and aggregate exposed to sulphate attack. *Const. Build. Mat.* 124, 705–713. <https://doi.org/10.1016/j.conbuildmat.2016.06.058>.
33. Santillán, L.R.; Villagrán-Zaccardi, Y.A.; Zega, C.J. (2018) Assessment of the influence of recycled aggregate on the resistance to external sulfate attack by accelerated testing of mortar bars. *Proceedings of 4th International Conference on Service Life Design for Infrastructures (SLD4), 27–30 August, Delft, Netherlands, RILEM Publications S.A.R.L.,* 793–802.
34. Li, Y.; Wang, R.; Li, S.; Zhao, Y.; Qin, Y. (2018) Resistance of recycled aggregate concrete containing low- and high-volume fly ash against the combined action of freeze-thaw cycles and sulfate attack. *Const. Build. Mat.* 166, 23–34. <https://doi.org/10.1016/j.conbuildmat.2018.01.084>.
35. Qi, B.; Gao, J.; Chen, F.; Shen, D. (2017) Evaluation of the damage process of recycled aggregate concrete under sulfate attack and wetting-drying cycles. *Const. Build. Mat.* 138, 254–262. <https://doi.org/10.1016/j.conbuildmat.2017.02.022>.
36. Dhir, R.K.; Limbachiya, M.C.; Leelawat, T. (1999) Suitability of Recycled Concrete Aggregate for Use in Bs 5328 Designated Mixes. *Proceedings of the Institution of Civil Engineers - Structures and Buildings, August 1999.* 134 [3], 257–274. <https://doi.org/10.1680/istbu.1999.31568>.
37. Bulatovic, V.; Melesev, M. (2017) Evaluation of sulfate resistance of concrete with recycled and natural aggregates. *Const. Build. Mat.* 152, 614–631. <https://doi.org/10.1016/j.conbuildmat.2017.06.161>.
38. Boudali, S.; Soliman, A.M.; Abdulsalam, B.; Kada, A. (2017) Microstructural Properties of the Interfacial Transition Zone and Strength Development of Concrete Incorporating Recycled Concrete Aggregate. *Int. Jour. of Struct. and Const. Eng.* 11 [8], 1012–1016. <https://doi.org/10.5281/zenodo.1131633>.
39. Somna, R.; Jaturapitakkul, C.; Made, A.M. (2012) Effect of ground fly ash and ground bagasse ash on the durability of recycled aggregate concrete. *Cem. Conc. Comp.* 34 [7], 848–854. <https://doi.org/10.1016/j.cemconcomp.2012.03.003>.
40. Arredondo-Rea, S.P.; Corral-Higuera, R.; Neri-Flores, M.A.; Gómez-Soberón, J.M.; Almeraya-Calderón, F.; Castorena-González, J.H.; Almaral-Sánchez, J.L. (2011) Electrochemical Corrosion and Electrical Resistivity of Reinforced Recycled Aggregate Concrete. *Int. J. Electrochemical Sci.* 6, 475–483. <http://www.electrochemsci.org/papers/vol6/6020475.pdf>.
41. Tangchirapat, W.; Khamklai, S.; Jaturapitakkul, C. (2012) Use of ground palm oil fuel ash to improve strength, sulfate resistance, and water permeability of concrete containing high amount of recycled concrete aggregates. *Mat. Design.* 41, 150–157. <https://doi.org/10.1016/j.matdes.2012.04.054>.
42. Rattanachu, P.; Tangchirapat, W.; Jaturapitakkul, C. (2019) Water Permeability and Sulfate Resistance of Eco-Friendly High-Strength Concrete Composed of Ground Bagasse Ash and Recycled Concrete Aggregate. *J. Mat. Civil Eng.* 31 [6]. [https://doi.org/10.1061/\(ASCE\)MT.1943-5533.0002740](https://doi.org/10.1061/(ASCE)MT.1943-5533.0002740).
43. Arredondo-Rea, S.P.; Corral-Higuera, R.; Almaral-Sánchez, J.L.; Castorena-González, M.A.; Neri-Flores, M.A.; Martínez-Villafañe, A. Almeraya-Calderon, F. (2009) Efficiency of Supplementary Materials Against Steel Corrosion in Concrete with Recycled Aggregate Exposed to Sulfates. *ECS Transactions.* 20 [1], 499–506. <https://doi.org/10.1149/1.3268417>.
44. Xie, J.; Zhao, J.; Wang, J.; Wang, C.; Huang, P.; Fang, C. (2019) Sulfate resistance of recycled aggregate concrete with GGBS and fly ash-based geopolymer. *Materials,* 12 [8], 1247. <https://doi.org/10.3390/ma12081247>.
45. Song, X.; Qiao, P.; Wen, H. (2015) Recycled aggregate concrete enhanced with polymer aluminium sulfate. *Mag. Concr. Res.* 67 [10], 496–502. <https://doi.org/10.1680/macrc.14.00119>.

46. Mendivil-Escalante, J.M.; Gómez-Soberón, J.M.; Almaral-Sánchez, J.L.; Cabrera-Covarrubias, F.G. (2017) Metamorphosis in the porosity of recycled concretes through the use of a recycled polyethylene terephthalate (PET) additive. Correlations between the porous network and concrete properties. *Materials*. 10 [2], 176. <https://doi.org/10.3390/ma10020176>.
47. Zega, C.J.; Coelho Do Santos, G.S.; Villagrán Zaccardi, Y.A.; Di Maio, A.A. (2016) Performance of recycled concretes exposed to sulphate soil for 10 years. *Construc. Build. Mat.* 102 [Part 1], 714–721. <https://doi.org/10.1016/j.conbuildmat.2015.11.025>.
48. IRAM 50001 (2000) Cemento. Cementos con propiedades especiales [Argentinian Standard. Cement. Cement with special properties].
49. UNE-EN 197 (2011). Cemento. Parte 1: Composición, especificaciones y criterios de conformidad de los cementos comunes.
50. ASTM C136-01 (2001) Standard test method for sieve analysis of fine and coarse aggregates, 5p.
51. ASTM C33-03 (2003) Standard specification for concrete aggregates, 11p.
52. ASTM C127-01 (2001) Standard test method for specific gravity and absorption of coarse aggregate, 5p.
53. ASTM C117-03 (2003) Standard test method for materials finer than 75- μ m (No. 200) sieve in mineral aggregates by washing, 4p.
54. ASTM C131-03 (2003) Standard test method for resistance to degradation of small-size coarse aggregate by abrasion and impact in the Los Angeles machine.
55. IRAM 1871 (2004) Hormigón. Método de ensayo para determinar la capacidad y la velocidad de succión capilar de agua del hormigón endurecido [Argentinian Standard. Concrete. Test method for the determination of the water capillary sorption capacity and rate of hardened concrete].
56. IRAM 1554 (1983). Hormigón. Método de determinación de la penetración de agua a presión en el hormigón endurecido [Argentinian Standard. Concrete. Test method for the determination of water penetration under pressure in hardened concrete].
57. BS-EN 12390-8 (2009) Testing hardened concrete. Depth of penetration of water under pressure.
58. ASTM C642-97 (1997) Standard test method for Density, Absorption, and Voids in Hardened Concrete, 3p.
59. Villagrán-Zaccardi, Y.A.; Egüez-Alava, H.; De Buysser, K.; Gruyaert, E.; De Belie, N. (2017) Calibrated quantitative thermogravimetric analysis for the determination of portlandite and calcite content in hydrated cementitious systems. *Mat. Struct.* 50 [3], 179. <https://doi.org/10.1617/s11527-017-1046-2>.
60. CIRSOC 201 (2005) Reglamento Argentino de Estructuras de Hormigón [Argentinian Standard, In Spanish].
61. Bonen, D.; Cohen, M.D. (1992) Magnesium sulfate attack on portland cement paste-I. Microstructural analysis. *Cem. Conc. Res.* 22 [1], 169–180. [https://doi.org/10.1016/0008-8846\(92\)90147-N](https://doi.org/10.1016/0008-8846(92)90147-N).
62. Santhanam, M.; Cohen, M.D.; Olek, J. (2002) Mechanism of sulfate attack: a fresh look - Part 1: Summary of experimental results. *Cem. Conc. Res.* 32 [6], 915–921. [https://doi.org/10.1016/S0008-8846\(02\)00724-X](https://doi.org/10.1016/S0008-8846(02)00724-X).
63. Schmidt, T.; Lothenbach, B.; Romer, M.; Neuenschwander, J.; Scrivener, K. (2009) Physical and microstructural aspects of sulfate attack on ordinary and limestone blended Portland cements. *Cem. Conc. Res.* 39 [12], 1111–1121. <https://doi.org/10.1016/j.cemconres.2009.08.005>.
64. Lothenbach, B.; Durdzinski, P.; De Weerd, K. (2016) Thermogravimetric analysis, In *Scrivener K, Snellings R, Lothenbach B (eds): A Practical Guide to Microstructural Analysis of Cementitious Materials, 1st edition. Boca Raton, USA: CRC Press.* 2016, 177–211.
65. Halle, J.C.; Stern, K.H. (1980) The effect of silica on the thermal decomposition of sodium sulphate. *Corrosion Science*. 20 [10], 1139–1142. [https://doi.org/10.1016/0010-938X\(80\)90144-4](https://doi.org/10.1016/0010-938X(80)90144-4).
66. González, M.; Irassar, E.F. (1998) Effect of limestone filler on the sulfate resistance of low C₃A Portland cement. *Cem. Conc. Res.* 28 [11], 1655–1667. [https://doi.org/10.1016/S0008-8846\(98\)00144-6](https://doi.org/10.1016/S0008-8846(98)00144-6).
67. Skalny, J.; Marchand, J.; Odler, I. (2002) Sulfate Attack on Concrete, London, UK: Spon, 2002.
68. Ferraris, C.F.; Stutzman, P.E.; Kenneth, S.A. (2006) Sulfate Resistance of Concrete: a new approach. *R&D Serial No. 2486, Skokie, Illinois: Portland Cement Association.* 2006, 93p.
69. Rasheeduzzafar (1992) Influence of Cement Composition on Concrete Durability. *ACI Materials Journal*. 89 [6], 574–586. <https://doi.org/10.14359/4033>.
70. Messad, S.; Carcassès, M.; Linger, L.; Boutillon, L. (2010) Performance Approach Using Accelerated Test Method for External Sulfate Attack. *Proceedings of the 3rd fib International Congress, 29 May to 2 June, Washington, USA.* 1–11.